Published in final edited form as:
J Pharmacol Exp Ther. 2009 March ; 328(3): 715–722. doi:10.1124/jpet.108.147330.

Microtubule Binding and Disruption and Induction of Premature Senescence by Disorazole C_1

Marni Brisson Tierno, **Carolyn A. Kitchens**, **Bethany Petrik**, **Thomas H. Graham**, **Peter Wipf**, **Fengfeng Xu**, **William Saunders**, **Brianne S. Raccor**, **Raghavan Balachandran**, **Billy W. Day**, **Jane R. Stout**, **Claire E. Walczak**, **Alexander P. Ducruet**, **Celeste E. Reese**, and **John S. Lazo**
Drug Discovery Institute (M.B.T., C.A.K.,B.P., P.W., B.W.D.,A.P.D.,C.E.R., J.S.L), Departments of Pharmacology (M.B.T., C.A.K., A.P.D. J.S.L), Chemistry (T.H.G., P.W.), Biological Sciences (F.X., W. S.) and Pharmaceutical Sciences (B.S.R., R. B., B.W.D), the Center for Chemical Methodologies and Library Development (P.W.), University of Pittsburgh, Pittsburgh, PA 15260; Medical Sciences Program, Indiana University, Bloomington, IN 47405 (J.R.S., C.E.W.)

Abstract

Disorazoles comprise a family of 29 macrocyclic polyketides isolated from the fermentation broth of the myxobacterium *Sorangium cellulosum.* The major fermentation product, disorazole A_1, was previously found to irreversibly bind to tubulin and to have potent cytotoxic activity against tumor cells, possibly due to its highly electrophilic epoxide moiety. To test this hypothesis, we synthesized the epoxide-free disorazole C_1 and found it retained potent antiproliferative activity against tumor cells, causing prominent G_2/M phase arrest and inhibition of *in vitro* tubulin polymerization. Furthermore, disorazole C_1 produced disorganized microtubules at interphase, misaligned chromosomes during mitosis, apoptosis, and premature senescence in the surviving cell populations. Using a tubulin polymerization assay, we found disorazole C_1 inhibited purified bovine tubulin polymerization with an IC_{50} of 11.8 ± 0.4 μM and inhibited [^{3}H]vinblastine binding uncompetitively with a K_i of 4.5 ± 0.6 μM. We also found uncompetitive inhibition of [^{3}H]dolastatin 10 binding by disorazole C_1 with a K_i of 10.6 ± 1.5 μM, indicating that disorazole C_1 bound tubulin uniquely among known antimitotic agents. Disorazole C_1 could be a valuable chemical probe for studying the process of mitotic spindle disruption and its relationship to premature senescence.

Introduction

Natural products have provided a plethora of pharmacologically useful drugs and chemical probes. The disorazole polyene macrodiolides were first isolated from the myxobacterium *Sorangium cellulosum* in 1994 and characterized to have significant antifungal activity with no antibacterial activity (Jansen et al., 1994). Initial biochemical and pharmacological studies were restricted to the major fermentation product, disorazole A_1 (Fig. 1), which blocks cell proliferation, causes G_2/M phase arrest and loss of microtubules, and induces apoptosis. Moreover, it blocks *in vitro* polymerization of tubulin (Elnakady et al., 2004; Kopp et al., 2005). Disorazole A_1 contains a highly electrophilic divinyl oxirane moiety that we hypothesized might mediate the mitotic arrest and inhibition of tubulin polymerization through covalent binding to tubulin (Wipf et al., 2006). The highly electrophilic divinyl oxirane of disorazole A_1 is generally not viewed as a therapeutically desirable moiety and, therefore, we

Corresponding author: John S. Lazo; Pittsburgh Molecular Libraries Screening Center, Department of Pharmacology, University of Pittsburgh Drug Discovery Institute, Biomedical Science Tower-3, Suite 10040, 3401 Fifth Avenue, University of Pittsburgh, Pittsburgh, PA 15260; Telephone: 412-648-9200; Fax: 412-648-2229; Email: lazo@pitt.edu.

[1]Tierno, M.B., Petrik, B., Nickischer, D. and Johnston, P. Application Note LC01612000, Thermo Scientific

synthesized the rare family member disorazole C_1 (Fig. 1), which is devoid of reactive groups. Remarkably, disorazole C_1 retained antimitotic activity (Wipf and Graham, 2004; Wipf et al., 2006). Structural analogs suggested that the functional group array of disorazole C_1 and its three-dimensional conformation were critical for biological activity but little is known about its mechanism of action. In the current comprehensive report, we demonstrate that disorazole C_1 has potent antiproliferative activity against a wide variety of human tumor cells, disrupts cellular microtubule integrity, blocks microtubule polymerization *in vitro*, binds tubulin in a unique manner, and causes apoptosis and premature cellular senescence, all attributes associated with a promising anticancer agent.

Methods

Cell culture reagents and proliferation assays

Cells were cultured in the following media supplemented with 10% fetal bovine serum (VWR, West Chester, PA): PtK2 rat kangaroo kidney epithelial cells in MEM-α; head and neck squamous cell carcinoma cell lines in DMEM; A549 and WI-38 fibroblasts in Basal Medium Eagle; UPCI:SCC103 in MEM; MDA-MB-231, PC-3 and 2008 in RPMI; and HCT116 in McCoy's 5A. Unless otherwise indicated all media, sera, and supplements were obtained from Invitrogen (Carlsbad, CA) and other reagents were from Sigma-Aldrich (St. Louis, MO).

Inhibition of growth was determined spectrophotometrically with 3-(4,5-dimethylthiazol- 2-yl)-2,5-diphenyltetrazolium bromide or by measuring fluorescence in live cells using an alamar blue-based assay (Promega, Madison, WI). Alternatively, in some studies we fixed cells in 3.7% formaldehyde and stained nuclei with 2 μg/ml Hoechst 33342 dye to quantify cells using an ArrayScan VTi (Thermo Fisher Scientific, Waltham, MA). The 50% growth inhibitory concentrations (IC_{50}) of test agents were calculated after a 72 h incubation. For reversibility studies, we treated A549 cells for 1 h with vehicle, 10 nM disorazole C_1 or 1 μM nocodazole. Cells were either continuously exposed to compound in complete medium or briefly (1 h) exposed to a compound, which was removed by washing 3X with complete medium. Live cells were counted by trypan blue exclusion and normalized to control cells. For studies with quiescent cell studies, confluent WI-38 cells were treated for 72 h with either DMSO or disorazole C_1.

Immunofluorescence detection of microtubules

PtK2 cells ($3x10^4$ cells/35 mm well) were plated 48 h prior to treatment. Cells were rinsed twice to remove antibiotics and incubated for 24 h with compounds diluted in antibiotic free growth medium. Cells were processed to visualize microtubules and DNA, and digital images were collected and manipulated as described previously (Stout et al., 2006). A549 cells were plated on coverslips in 6 well plates for 24 h before compound treatment, fixed in 3.7% paraformaldehyde, and incubated in 0.1% Triton X-100 at 4° C for 7 min. A 1% solution of BSA in PBS plus 0.1% Tween was used as the blocking buffer. Microtubules were visualized using an anti-α-tubulin mouse monocolonal antibody (Abcam) with goat-anti-mouse Alexa Fluor488 (Invitrogen) secondary antibody diluted in 1% BSA/PBS plus 0.1% Tween. Nuclei were visualized with the fluorescent dye 4,6-diamidino-2- phenylindole and an Olympus BX60 epifluorescence microscope. Images were taken using a Hamamatsu Argus-20 CCD camera and image processor (Hamamatsu Co., Bridgewater, NJ).

Radioligand binding and inhibition of tubulin assembly

Tubulin was isolated from bovine brain as previously described (Hamel and Lin, 1984). [^{3}H] Vinblastine (specific activity 61–315 mCi/mmol) and Sephadex G-50 were from GE Healthcare (Piscataway, NJ). Handee centrifuge columns and the bicinchoninic acid protein assay kit were from Pierce Biotechnology (Rockford, IL). [^{3}H]Dolastatin 10 (specific activity

26–133 mCi/mmol), dolastatin 10, and paclitaxel were from the Drug Synthesis and Chemistry Branch at the National Cancer Institute (Rockville, MD). Radiolabeled ligand binding to tubulin was measured by centrifugal gel filtration and scintillation spectrometry as previously described (Bai et al., 1995b) with minor modifications (Wang et al., 2007). The average stoichiometry of binding in the control reaction mixture was 0.63 moles of [^{3}H]vinblastine or [^{3}H]dolastatin 10/mole of tubulin. For the tubulin assembly studies, we used homogeneous bovine brain tubulin (10 μM) and previously described methods (Wang et al., 2007).

Apoptosis and senescence assays

A549 cell were analyzed for apoptosis using a commercially available fluorescein terminal dUTP nick-end labeling (TUNEL) method with fluorescence microscopy as described by the manufacturer (Roche In Situ Cell Death Kit). For senescence measurements A549 cells (3.5 x 10^5 cells/well) were plated 24 h prior to treatment with DMSO vehicle or test compounds for 1–7 days. For 7 day treatments, individual wells were split on day 3 or 4 to avoid the cultures reaching confluency. β-Galactosidase staining was performed as previously described (Dimri et al., 1995) and quantified both by visual counting by a naïve observer or by acquiring images with the brightfield module on an ArrayScan VTI and using the Cellomics Compartmental Analysis V3 Bioapplication to define cells with positive β-galactosidase staining (mean of 20 acquired fields/well). For BrdU incorporation, A549 cells were pretreated in thymidine-free medium, incubated for 6 h with BrdU, and visualized using a cell proliferation kit (GE Healthcare, Piscataway, NJ). BrdU images were acquired (20 fields/well) with an ArrayScan VTi and analyzed using the Cellomics Compartmental Analysis V3 Bioapplication to determine the percentage of cells with fluorescence greater than the set threshold and to quantify BrdU positive cells. For Western blotting, A549 cells were treated with compounds for 7 days as stated above followed by cell harvesting in ice cold lysis buffer (50 mM Tris, pH 7.6, containing 150 mM NaCl, 1 mM EDTA, 0.1% SDS and 1% Triton X-100) supplemented with protease and phosphatase inhibitors. Protein concentrations in cell lysates were determined with the BCA protein assay kit (Promega). Individual proteins were detected by standard Western blotting methods with the following antibodies: p53, pRb, phospho-Rb (ser780), γH2AX, and GAPDH antibodies (Cell Signaling, Danvers, MA); p21 antibody (EMD Biosciences); vinculin (Santa Cruz Biotech, Santa Cruz, CA); cyclin D antibody (BD Biosciences, San Jose, CA). Discodermolide was obtained from Norvartis A.G. (Basel, Switzerland) and disorazole A1 was from Æterna Zentaris (Frankfurt am Main, Germany).

Results

Disorazole C_1 is a potent inhibitor of cell proliferation, interferes with tubulin polymerization, and binds to tubulin

As an extension of our previous study with HeLa cells (Wipf et al., 2006), we examined the growth inhibitory activity of disorazole C_1 using 11 other human tumor carcinoma cell lines (Table 1). Disorazole C_1 was remarkable potent with an average 50% growth inhibitory concentration (IC_{50}) of 1.7 ± 0.6 nM (SEM). Head and neck cancer cell lines were particularly sensitive to disorazole C_1 with an average IC_{50} value of 358 ± 56 pM. The p53 wild type HCT116 cells exhibited similar sensitivity to disorazole C_1 compared to the p53 null MDA-MB-231 cells. When quiescent WI-38 fibroblasts were exposed to disorazole C_1 for 72 h, we observed no change in cell number or morphology. In contrast proliferating WI-38 cells were sensitive to disorazole C_1, indicating that active cell division was important for the cytotoxic effects of disorazole C_1.

Disorazole A_1 was previously reported to inhibit tubulin polymerization *in vitro* at substoichiometric concentrations and block cell proliferation at the G_2/M phase (Elnakady et al., 2004). We previous observed disorazole C_1 caused G_2/M phase arrest with HeLa cells

(Wipf et al., 2006). As illustrated in Figure 2A disorazole C_1 clearly disrupted GTP-mediated tubulin assembly in a concentration-dependent manner with an IC_{50} of 11.8 ± 0.4 μM (Fig. 2A), indicating a compound:tubulin stoichiometry of approximately 1:1.

We next probed the ability of disorazole C_1 to inhibit the binding of [^{3}H]vinblastine or [^{3}H] dolastatin 10 to purified tubulin as previously described (Bai et al., 1995b) (Fig. 2B and 2C). As illustrated by the intersecting lines in the Hanes-Woolf plot (Fig. 2B), disorazole C_1 inhibited [^{3}H]vinblastine binding in an uncompetitive manner with a K_i of 4.5 ± 0.6 μM. With this linear transformation the lines would be parallel if the inhibition was competitive. Dolastatin 10 binds at the depsipeptide binding site on tubulin, which overlaps with the vinca alkaloids binding site (Bai et al., 1995a; Bai et al., 1995b). Interestingly, we also found uncompetitive inhibition of [^{3}H]dolastatin 10 binding by disorazole C_1 with a K_i of 10.6 ± 1.5 μM, suggesting that disorazole C_1 might bind tubulin uniquely among known antimitotic agents.

We next treated A549 cells with IC_{50} concentrations of disorazole C_1 or vinblastine and visualized microtubule integrity by immunofluorescence microscopy (Fig. 3). Compared to vehicle control, disorazole C_1 disrupted microtubules as early as 24 h (Fig. 3b) with complete disruption within 72 h (Fig. 3c). Even within 1 h, disorazole C_1 (2 nM, 3f; 10 nM, 3g; 20 nM, 3h) and vinblastine (20 nM, 3i) caused a dissolution of microtubules.

To further assess the effects of disorazole C_1 on microtubules at interphase and mitosis, we examined PtK2 rat kangaroo kidney epithelial cells, which are widely used to study antimitotics because they have a flat morphology and large chromosomes allowing greater visualization. PtK2 cells were treated for 24 h in the presence of disorazole C_1 (5, 25 or 100 nM) or the inactive but structurally closely related analog O1OA (Fig. 1). O1OA had no effect on microtubules at interphase or mitosis where chromosomes aligned normally along the metaphase plate (Fig. 4). In contrast, disorazole C_1 completely disrupted microtubules at both concentrations. At mitosis, complete misalignment of chromosomes was evident as were multipolar spindles and dispersed chromosomes with no attached microtubules. These results in combination with the data described in Figure 3 confirmed that disorazole C_1 treatment had a dramatic effect on cellular microtubules, causing disruption of normal mitotic processes.

We next determined the durability of the growth inhibitory effects of disorazole C_1. A549 cells were treated for 1 h with 10 nM disorazole C_1, 1 μM nocodazole or DMSO vehicle and were maintained in medium containing compound (contin) or washed and maintained in medium lacking compound (wash) and incubated for 1–144 h (Fig. 5A). The cytotoxic effects of nocodazole, a reversible inhibitor of mitosis, were completely reversed with compound washout. In contrast, cell viability continued to decline during the 72 h in cultures exposed briefly (1 h) or continuously to 10 nM disorazole C_1. The number of surviving cell remained relatively constant between 72 and 144 h, suggesting growth arrest and possible senescence. A microscopic analysis of microtubule integrity also suggested the disorazole C_1-mediated microtubule disruption was not readily reversible. Furthermore, the IC_{50} values for cells treated for 1 h or 7 days were similar (2.2 vs 1.5 nM). These growth inhibitory results were consistent with a previous report using disorazole A_1 in which the cytotoxic effects were prolonged (Elnakady et al., 2004). Disorazole C_1 at 10 nM caused some apoptosis in A549 cells (Fig. 5B), although it was much less effective to what has been reported for disorazole A_1 (Elnakady et al., 2004). Thus, treatment of A549 cells with 2 nM disorazole C_1 for 24 or 48 h caused no significant apoptosis as detected by a TUNEL assay, although treatment with 10 nM for 48 h did cause detectable apoptosis (Fig. 5B). These results indicate that the highly reactive vinyl oxirane subunit in disorazole A_1 was dispensable for the prolonged cytotoxicity caused by the disorazole family members.

Disorazole C_1 induces premature senescence

Because drug-resistant cells have been so valuable in understanding the mechanism of action of new small molecules, we attempted to generate A549 cells that were resistant to disorazole C_1 using chronic exposure to increasing compound concentrations in culture. Although our initial efforts were unsuccessful, when we examined the population that survived a one week exposure, we observed cells with an enlarged, flattened morphology. These cells ceased to divide but remained viable for >50 days in the presence or absence of disorazole C_1. We tested whether or not these cells entered premature senescence using a classic β-galactosidase staining procedure at pH 6.0 after treatment of A549 cells for 7 days with 1–10 nM disorazole C_1 (Fig. 6). Cells treated with DMSO or the inactive O1OA analog displayed only a few sparse β-galactosidase positive cells whereas the positive control, doxorubicin, showed abundant β-galactosidase staining at the IC_{50} concentration of 50 nM. Cells treated with an IC_{50} concentration of discodermolide also displayed high levels of β-galactosidase positive cells while an equipotent growth inhibitory concentration of vinblastine had no effect consistent with previous results (Chang et al., 1999;Klein et al., 2005). Disorazole C_1 treatment resulted in positive β-galactosidase staining even at concentrations below the growth IC_{50} (1 nM). The percentage of β-galactosidase positive cells with disorazole C_1 treatment was comparable to that seen with doxorubicin. Disorazole C_1 also produced positive β-galactosidase human colon cancer (HCT116), lung cancer (H1299), and oral squamous carcinoma (UPCI:SCC103) cells, but not PC-3 prostate cancer cells (data not shown).

Alterations in the protein expression profiles of some of the classic markers of premature senescence also supported the hypothesis that these metabolically active, non-dividing cells had indeed undergone premature senescence. A549 and HCT116 cells were treated for 7 days with concentrations of doxorubicin (50 nM), disorazole C1 (2 nM), discodermolide (25 nM), or vinblastine (2 nM) that had equivalent growth inhibition. Cells were lysed, protein was isolated and the protein expression was determined by Western blotting (Fig. 6B). All compounds increased the levels of cyclin dependent kinase inhibitor p21 and cyclin D. Lower levels of Ser780 phosphorylated pRb and total pRb levels were also observed as expected for cells undergoing cell cycle arrest and premature senescence. Vinblastine (2 nM) also induced p53, p21, Rb and cyclin D consistent with cell cycle arrest and senescence, although little β-galactosidase staining was observed (Fig. 6 and 7).

Further documenting the role of microtubule disruption in premature senescence, observed DNA synthesis as measured by BrdU incorporation was inhibited by 67% in A549 cells treated for 1 day with IC_{50} concentration of disorazole C_1 (2 nM), which was equivalent to that seen with the 50% growth inhibitory concentration of doxorubicin (50 nM) (Fig. Supplemental Fig. 1 and Supplemental Table 1). In contrast, almost all cells incorporated BrdU after treatment with the inactive analog O1OA, vinblastine, discodermolide or DMSO vehicle control, indicating actively dividing cells. By 7 days, almost no cells were actively dividing after treatment with doxorubicin, discodermolide or disorazole C_1 ($\geq$ 0.5 nM) (Supplemental Fig. 1 and Supplemental Table 1). Some decrease in BrdU positive cells was seen after a week of treatment with either 10 nM O1OA or 2 nM vinblastine. We also excluded the possibility that the induction of premature senescence was the product of double-strand DNA breaks, since we did not detect an increase in Ser139 phosphorylation of γH2AX after treatment with either disorazole C_1 or vinblastine (Supplemental Fig. 2). These results in combination with the positive β-galactosidase staining and changes in cell cycle protein markers indicate that disorazole C_1 could induce premature senescence in some human tumor cells.

Discussion

The highly electrophilic divinyl oxirane moiety of disorazole A_1 has been an attractive candidate mediator for the inhibition of tubulin polymerization and our results indicate that at

least some of the pharmacological activity of the disorazole family resides in other aspect of the disorazole pharmacophore. The disorazole C_1 concentration required to inhibit tubulin polymerization by 50% *in vitro* (namely, 11.8 μM) was approximately an order of magnitude higher than the IC_{50} values reported for disorazole A_1 (1.8 μM) using a similar assay (Elnakady et al., 2004). Our *in vitro* tubulin binding studies indicated that disorazole C_1 had a unique direct tubulin binding interaction possibly binding at or near a site typically occupied by vinblastine and dolastain 10. We could not, however, rule out the possibility that disorazole C_1 bound to a completely unrelated site on tubulin, instigating a conformational change that allosterically interferes with vinblastine and dolastatin-10 binding. Further studies are needed to determine the exact binding domain of disorazole C_1 on tubulin. These results indicate disorazole C_1, like disorazole A_1 (Elnakady et al., 2004), inhibited microtubule polymerization in the absence of abundant microtubule associated proteins.

Disorazole C_1 prevented proper assembly of microtubules within cells. The disorazole C_1 concentration required to inhibit tubulin polymerization by 50% *in vitro* would be expected to be higher because the concentration of purified tubulin (10 μM) used in the *in vitro* reactions was intentionally high to permit robust detection. Moreover, it is now recognized that most effective anticancer drugs affect microtubule depolymerization or polymerization at much lower concentrations than required for *in vitro* studies (Jordan and Wilson, 2004). The lower concentration of disorazole C_1 or A_1 required to disrupt cellular proliferation likely reflected the need to affect only a small fraction of the tubulin/microtubule dynamics to block the cell division machinery. The breakdown of microtubules was seen as early as 15 min after a 5 nM disorazole C_1 treatment, with complete absence of cells with visible microtubules within 4 h (data not shown). We speculate that the long-lived disorazole C_1 cytotoxicity might be due to misalignment of chromosomes at the metaphase plate consistent with the G_2/M arrest and increase in mitotic index that we previously described (Wipf et al., 2006). All of these data indicated that disorazole C_1 was a potent, cytotoxic, microtubule destabilizer that prevents normal cell division. Nonetheless, the previously reported IC_{50} values for growth inhibition with disorazole A_1 suggest it is even more potent than disorazole C_1 probably because of the highly reactive divinyl oxirane moiety. Indeed, in preliminary growth inhibition studies with Hela cells we observed an IC_{50} of 47 pM for disorazole A_1 compared to an IC_{50} of 219 pM for disorazole C_1. It remains to be determined if disorazole C_1 has a better therapeutic potential compared with the more potent disorazole A_1.

Proliferating cells that are subjected to significant harmful stress rapidly exit the cell cycle through several concurrent failsafe “checkpoint” mechanisms enabling DNA repair and suppressing possible tumorigenesis. If these cell-cycle checkpoints are deficient due to the presence of mutations or overwhelming damage, cells generally engage in apoptosis or senescence. Senescence is defined as permanent cell-cycle arrest preventing proliferation but permitting metabolic activity. Senescent cells have an enlarged, flattened morphology with an increased cytoplasmic area, increased granularity, extensive cytoplasmic vacuoles and multinucleation (Schmitt, 2007). There currently is no single accepted biochemical defining marker for the senescence phenotype, although perinuclear lysosomal presence of β-galactosidase is often considered to be a senescence characteristic (Dimri et al., 1995). In addition, senescent cells do not synthesize DNA and therefore display decreased BrdU uptake. Cells undergoing senescence show changes in the expression of genes involved in tumor suppression, cell cycle progression, mitosis and DNA replication. Thus, the tumor suppressor protein p53, which upregulates the cyclin-dependent kinase inhibitors p21 and p16, is activated and promotes growth arrest in cells undergoing senescence (Stein et al., 1999; Roninson, 2003; Serrano, 2007). The proliferation blockage associated with senescence appears to be irreversible since few cells actually recover from prolonged upregulation of tumor suppressors, such as p53, p21, and p16.

Chemotherapy-induced senescence has been reported with mechanistically distinct agents including DNA alkylators, antimetabolites, topoisomerase inhibitors, irradiation, and some microtubule stabilizers (Chang et al., 1999; Klein et al., 2005; Schmitt, 2007). Senescence is typically induced at low drug concentrations whereas high concentrations produce overwhelming damage that favor apoptosis. For example, treatment of human hepatoma cells with a low concentration of the indirect DNA damaging agent doxorubicin (<100 nM) induces senescence, eventually leading to mitotic catastrophe, whereas a high concentration (20 μM) leads to apoptosis (Eom et al., 2005). Considering the broad mechanisms of action of the anticancer agents causally involved in tumor cell senescence, it is surprising that in initial studies clinically important inhibitors of tubulin polymerization, such as vinblastine and vincristine, were not observed to be potent inducers of senescence (Chang et al., 1999; Schmitt, 2007) even though one would hypothesize that kinetochore stress imposed by mitotic spindle checkpoints might lead to senescence (Yamada and Gorbsky, 2006). Interestingly, recent work by Arthur and coworkers (Arthur et al., 2007) suggests that the inhibitor of microtubule polymerization, JG-03-14, caused senescence in residual surviving cell populations. Treatment of L929 mouse fibroblasts and PtK2 rat kangaroo kidney epithelial cells for 5 days with disorazole A_1 caused enlarged cells with increased metabolic activity that ceased to divide, possibly indicating that these surviving cells adopted a senescence phenotype (Elnakady et al., 2004). We found positive β-galactosidase staining in cells treated with disorazole C_1 at concentrations well below the IC_{50}. Prominent β-galactosidase staining was not observed previously with vinblastine (Lee et al., 2006), which no doubt contributed to the current belief that inhibition of microtubule polymerization does not provide a signal for senescence (Schmitt, 2007). Indeed, we also did not observe significant β-galactosidase expression in cells treated with vinblastine or vincristine at their IC_{50} concentrations for growth inhibition. It is also important to note, however, that β-galactosidase expression has been questioned as a marker for senescence (Lee et al., 2006). Thus, we examine additional markers including increased p53 and p21 with downregulation in total Rb and phospho-Rb consistent with senescence. A549 cells do not express another common marker of senescence, $p16^{INK4}$, rather they use p21 to maintain cell cycle arrest and senescence (Kashiwabara et al., 1998; McConnell et al., 1998). We saw increases in the levels of cyclin D while the cyclin dependent kinase inhibitor p21 was also elevated. It has been suggested that this phenomenon occurs due to hypermitogenic senescence, where supraphysiologic levels of mitogens (Ras/Raf/MAPK) increase cyclin D levels (Blagosklonny, 2003), but to date our efforts to identify activation of the MAPK pathway have not been successful. Finally, another marker of senescence is inhibition of DNA synthesis, which was markedly decreased in cells exposed to disorazole C_1 as early as 24 h after treatment with low concentrations (≥ 0.5 nM); both discodermolide and vinblastine were less efficacious.

In summary, our data provide evidence that microtubule destabilization can suppress cancer cell growth by inducing premature senescence at concentrations at or below the IC_{50} for growth inhibition. Other microtubule destabilizing agents, namely JG-03-14, also are reported to cause premature senescence (Arthur et al., 2007) albeit at higher concentrations (namely 500 nM, which causes 70–80% growth inhibition) than that required with disorazole C_1. These results illustrate microtubule disruption, like some other forms of cellular stress, provide intracellular signals promoting premature senescence at least in some tumor cell types. The propensity of disorazole C_1 to promote senescence may be related to the prolonged cellular effects or the nature of its interactions with microtubules. The availability of the previous asymmetrical synthesis of disorazole C_1 (Wipf and Graham, 2004; Wipf et al., 2006) places it in a ideal position for the production of radiolabeled compound and analog development. We speculate that disorazole C_1 could be a potent and valuable chemical probe for studying the process of premature senescence induced by mitotic spindle disruption.

Supplementary Material

Refer to Web version on PubMed Central for supplementary material.

Acknowledgements

We thank Drs. Jennifer Grandis (University of Pittsburgh) and June Biedler (Memorial Sloan Kettering) for providing the head and neck carcinoma and Chinese hamster lung cell lines, respectively; Drs. Kenneth Bair and Fred Kinder at Novartis AG (Basel, Switzerland) for providing the discodermolide; and Dr. Eckhard Günther at Æterna Zentaris (Frankfurt am Main, Germany) for providing disorazole A_1.

This work was supported by grants from the NIH CA078039 and CA097190 (SPORE in Head and Neck Cancer), the Fiske Drug Discovery Fund, and the METACyt Initiative of Indiana University (partially funded through a grant from the Lilly Endowment, Inc.).

Abbreviations

TUNEL

terminal dUTP nick-end labeling

References

Arthur CR, Gupton JT, Kellogg GE, Yeudall WA, Cabot MC, Newsham IF, Gewirtz DA. Autophagic cell death, polyploidy and senescence induced in breast tumor cells by the substituted pyrrole JG-03-14, a novel microtubule poison. Biochem Pharm 2007;74:981–991. [PubMed: 17692290]

Bai R, Taylor GF, Cichacz ZA, Herald CL, Kepler JA, Pettit GR, Hamel E. The spongistatins, potently cytotoxic inhibitors of tubulin polymerization, bind in a distinct region of the vinca domain. Biochem 1995a;34:9714–9721. [PubMed: 7626642]

Bai R, Taylor GF, Schmidt JM, Williams MD, Kepler JA, Pettit GR, Hamel E. Interaction of dolastatin 10 with tubulin: induction of aggregation and binding and dissociation reactions. Mol Pharmacol 1995b;47:965–976. [PubMed: 7746283]

Blagosklonny MV. Cell senescence and hypermitogenic arrest. EMBO reports 2003;4:358–362. [PubMed: 12671679]

Chang BD, Broude EV, Dokmanovic M, Zhu H, Ruth AC, Xuan Y, Kandel ES, Lausch E, Christov K, Roninson IB. A senescence-like phenotype distinguishes tumor cells that undergo terminal proliferation arrest after exposure to anticancer agents. Cancer Res 1999;59:3761–3767. [PubMed: 10446993]

Dimri GP, Lee X, Basile G, Acosta M, Scott G, Roskelley C, Medrano EE, Linskens M, Rubel I, Pereira-Smith O, Peacocke M, Campisi J. A biomarker that identifies senescent human cells in culture and in aging skin in vivo. Proc Natl Acad Sci USA 1995;92:9363–9367. [PubMed: 7568133]

Elnakady YA, Sasse F, Lunsdorf H, Reichenbach H. Disorazol A1, a highly effective antimitotic agent acting on tubulin polymerization and inducing apoptosis in mammalian cells. Biochem Pharmacol 2004;67:927–935. [PubMed: 15104246]

Eom Y-W, Kim MA, Park SS, Goo MJ, Kwon HJ, Sohn S, Kim W-H, Yoon G, Choi KS. Two distinct modes of cell death induced by doxorubicin:apoptosis and cell death through mitotic catastrophe accompanied by senescence-like phenotype. Oncogene 2005;24:4765–4777. [PubMed: 15870702]

Hamel E, Lin CM. Separation of active tubulin and microtubule-associated proteins by ultra centrifugation and isolation of a component causing the formation of microtubule bundles. Biochem 1984;23:4173–4184. [PubMed: 6487596]

Jansen R, Irschik H, Reichenbach H, Wray V, Hofle G. Disorazoles, highly cytotoxic metabolites from the sorangicin producing bacterium Sorangium cellulosum, strain So ce1. Liebigs Ann Chem 1994:759–773.

Jordan MA, Wilson L. Microtubules as a target for anticancer drugs. Nature Rev Cancer 2004;4:253–265. [PubMed: 15057285]

Kashiwabara K, Oyama T, Sano T, Fukuda T, Nakajima T. Correlation between methylation status of the p16/CDKN2 gene and the expression of p16 and Rb proteins in primary nonsmall cell lung cancers. Int J Cancer 1998;79:215–220. [PubMed: 9645340]

Klein LE, Freeze BS, Smith AB, Horwitz SB. The microtubule stabilizing agent discodermolide is a potent inducer of accelerated cell senescence. Cell Cycle 2005;4:501–507. [PubMed: 15711127]

Kopp M, Irschik H, Pradella S, Mueller R. Production of the tubulin destabilizer disorazol in Sorangium cellulosum: biosynthetic machinery and regulatory genes. Chembiochem 2005;6:1277–1286. [PubMed: 15892181]

Lee BY, Han JA, Im JS, Morrone A, Johung K, Goodwin EC, Kleijer WJ, DiMaio D, Hwang ES. Senescence-associated beta-galactosidase is lysosomal beta-galactosidase. Aging Cell 2006;5:187–195. [PubMed: 16626397]

McConnell BB, Starborg M, Brookes S, Peters G. Inhibitors of cyclin-dependent kinases induce features of replicative senescence in early passage human diploid fibroblasts. Curr Biol 1998;8:351–354. [PubMed: 9512419]

Roninson IB. Tumor cell senescence in cancer treatment. Cancer Res 2003;63:2705–2715. [PubMed: 12782571]

Schmitt CA. Cellular senescence and cancer treatment. Biochim Biophys Acta 2007;1775:5–20. [PubMed: 17027159]

Serrano M. Cancer regression by senescence. New Engl J Med 2007;356:1996–1997. [PubMed: 17494935]

Stein GH, Drullinger LF, Soulard A, Dulic V. Differential roles for cyclin-dependent kinase inhibitors p21 and p16 in the mechansisms of sensecence and differentiation in human fibroblasts. Mol Cell Biol 1999;19:2109–2117. [PubMed: 10022898]

Stout JR, Rizk RS, Kline SL, Walczak CE. Deciphering protein function during mitosis in PtK cells using RNAi. BMC Cell Biol 2006;7:26. [PubMed: 16796742]

Wang Z, McPherson PA, Raccor BS, Balachandran R, Zhu G, Day BW, Vogt A, Wipf P. Structure-activity and high-content imaging analyses of novel tubulysins. Chem Biol Drug Des 2007;70:75–86. [PubMed: 17683369]

Wipf P, Graham TH. Total synthesis of (-)-disorazole C1. J Am Chem Soc 2004;126:15346–15347. [PubMed: 15563138]

Wipf P, Graham TH, Vogt A, Sikorski RP, Ducruet AP, Lazo JS. Cellular analysis of disorazole C and structure-activity relationship of analogs of the natural product. Chem Biol Drug Des 2006;67:66–73. [PubMed: 16492150]

Yamada HY, Gorbsky GJ. Spindle checkpoint function and cellular sensitivity to anitmitotic drugs. Molec Cancer Therap 2006;5:2963–2970. [PubMed: 17172401]

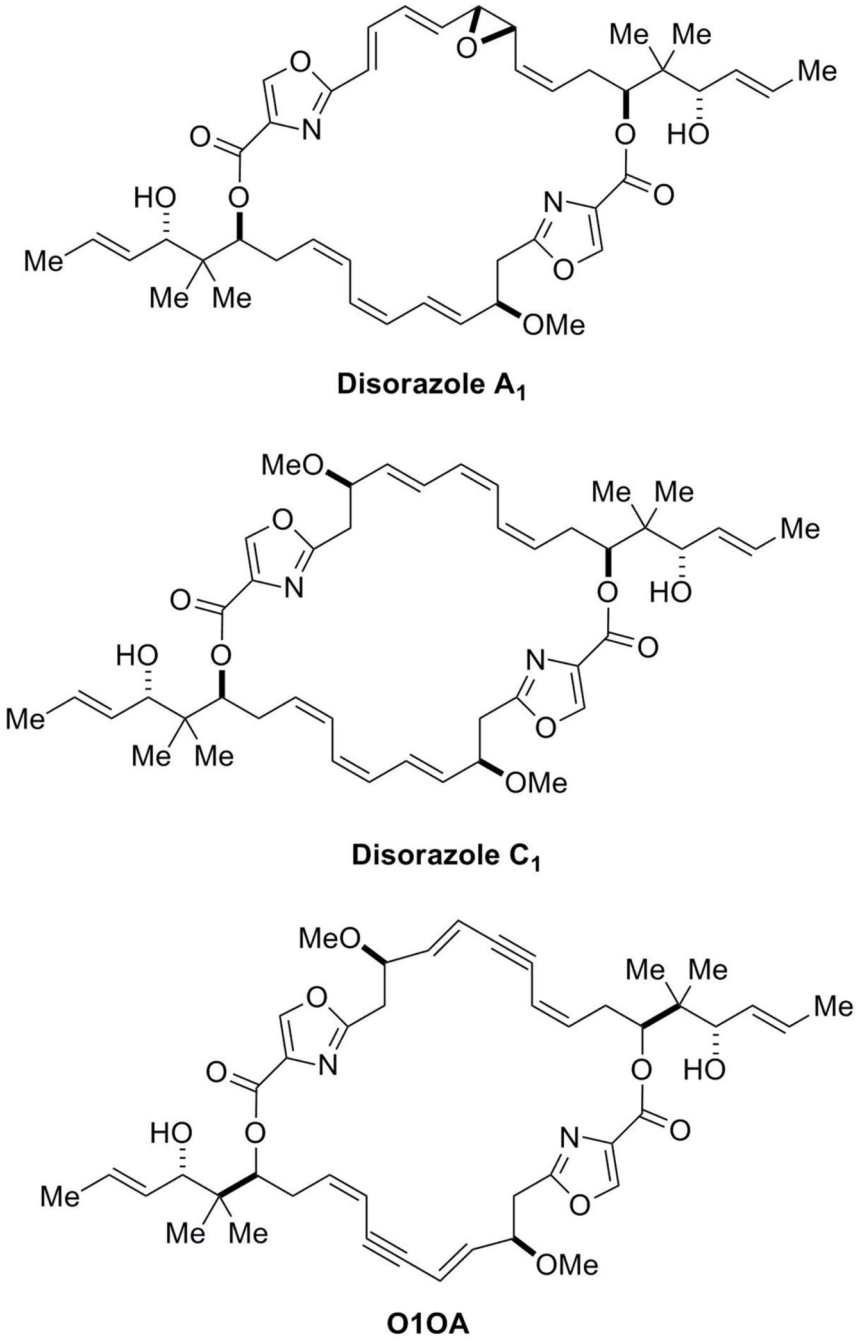

Figure 1.
Chemical structures of disorazoles.

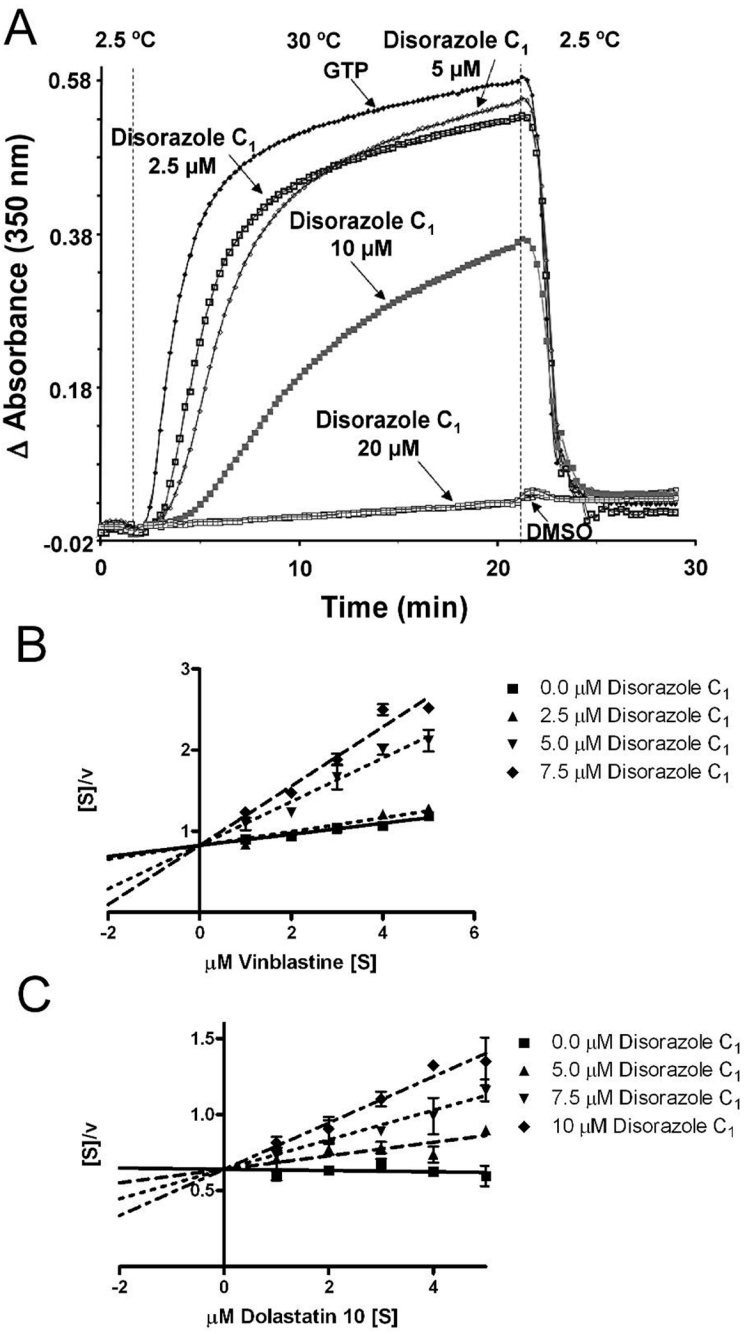

Figure 2. Disorazole C_1 disrupts microtubule assembly and binds to tubulin in vitro

(A) Bovine brain tubulin was preincubated with disorazole C_1 or vehicle and monosodium glutamate for 15 min at 30° C. The reaction mixture was cooled to 0° C, GTP was added, reaction mixtures were transferred to cuvettes, held at 2.5° C in a spectrophotometer and absorbance (turbidity) read at 350 nm. After a baseline was established, the temperature was raised to 30° C (~1 min). After 20 min, the temperature was returned to 2.5° C. GTP alone (no test compound) was assigned as 100% assembly (positive control) and DMSO alone (no test compound, no GTP) as 0% assembly (negative control). Hanes-Woolf plot of disorazole C_1 inhibition of [^{3}H]vinblastine (B) or [^{3}H]dolastatin 10 (C) binding to 10 μM bovine brain tubulin. The mixtures were incubated for 30 min at room temperature and bound versus free

radiolabeled ligand was separated using Sephadex G-50 columns. The amount of radiolabeled ligand bound to tubulin was determined using scintillation spectrometry. The substrate concentration [S] is indicated on the abscissa and the ration of the substrate concentration to the reaction velocity [v] indicated on the ordinate.

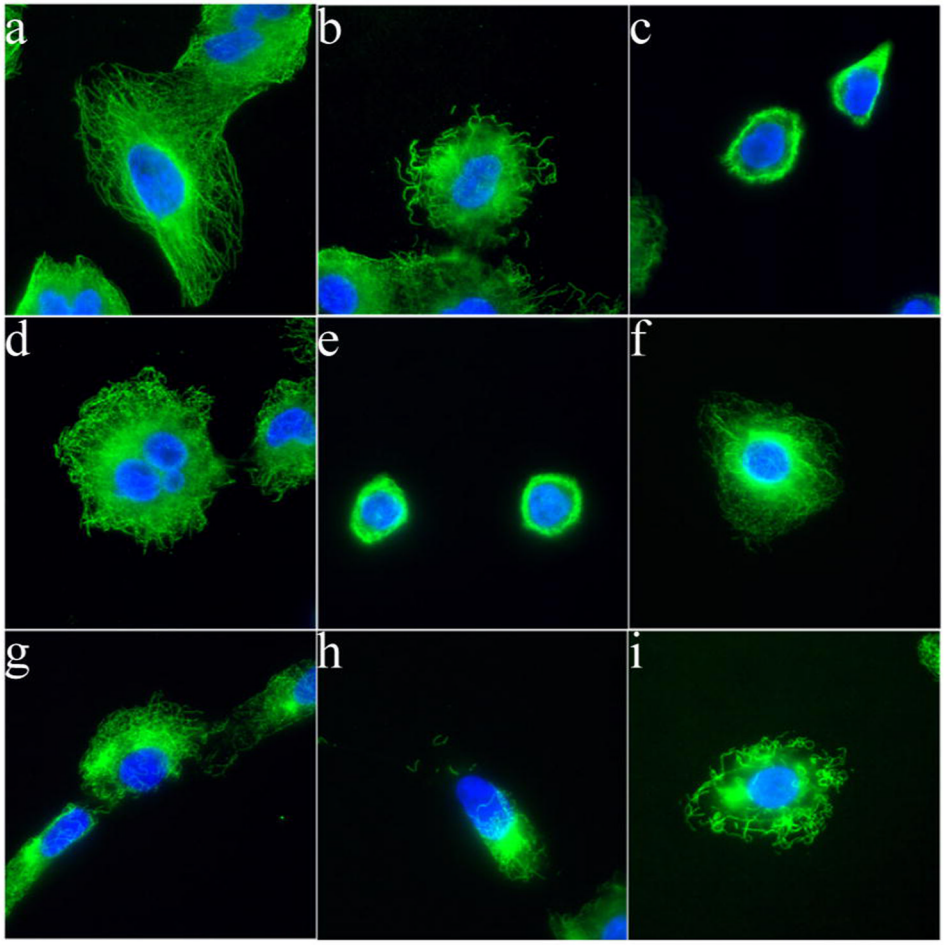

Figure 3. Disorazole C_1 disrupts microtubules *in vivo*

Microtubules in A549 cells were partially disrupted after disorazole treatment at 2 nM for 24 h (b) and more completely at 72 h (c) as compared to DMSO vehicle control (a). The disruption was similar to that seen with 2 nM vinblastine treatment at 24 h (d) and 72 h (e). A concentration response effect on microtubules after a 1 h treatment was observed with 2 nM (f), 10 nM (g) and 20 nM (h) disorazole C_1 similar to 20 nM vinblastine (i). With both compounds, apparent tubulin aggregation was observed at higher concentrations (h, i). Cells were fixed and stained with anti-α-tubulin antibody to visualize microtubules (green) and DAPI to visualize nuclei (blue).

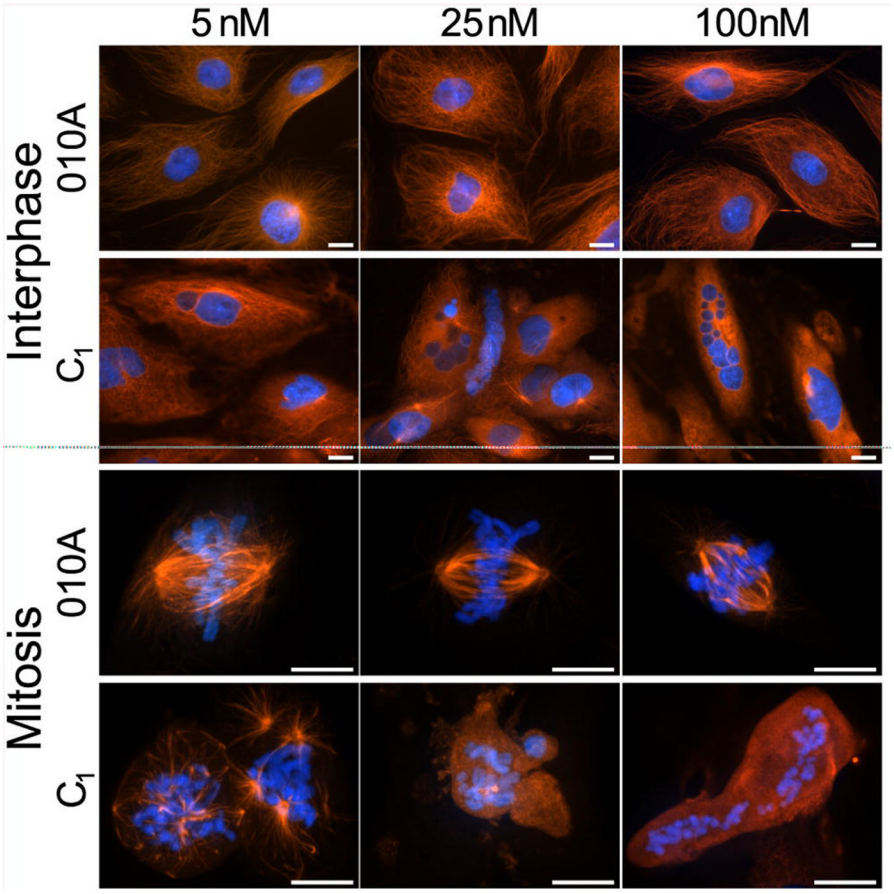

Figure 4. Disorazole C_1 disrupts microtubules at interphase and metaphase

Mammalian PtK2 cells were treated with the indicated concentrations of either O1OA (inactive analog of disorazole C_1) or disorazole C_1 for 24 h at 37°C. Cells were fixed and stained with anti-α-tubulin antibody to visualize microtubules (red) and Hoechst 33342 to visualize chromosomes (blue). All images were collected with a Nikon E600 microscope equipped with a Roper CoolSnap HQ digital camera at 40X (interphase) or 100X objectives (mitotic spindles). Upper panels, interphase; lower panels, mitosis. Bars = 10 μm.

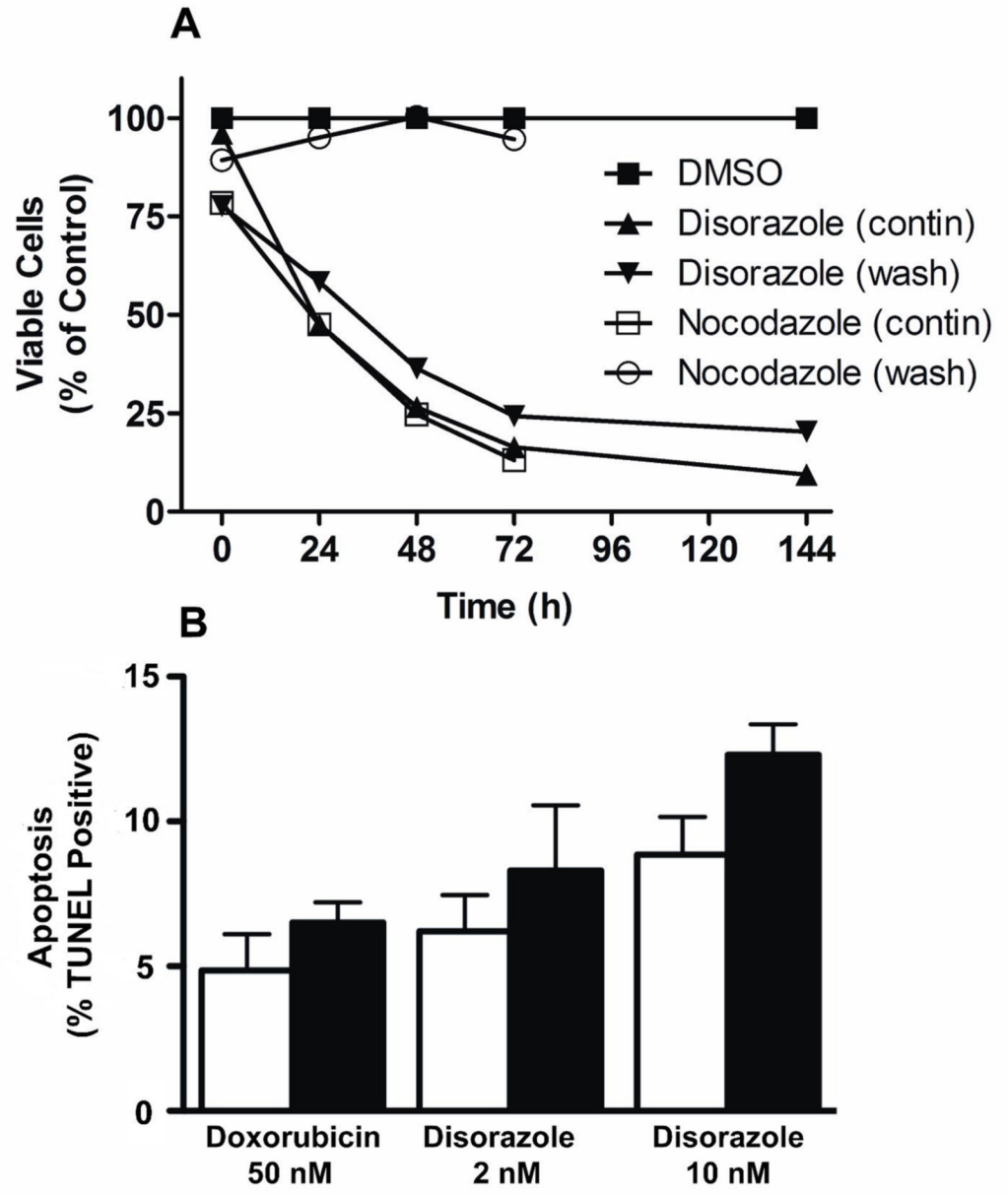

Figure 5. Disorazole C_1 causes irreversible growth inhibition

A549 cells were treated for 1 h with 10 nM disorazole C_1, 1 μM nocodazole or DMSO vehicle followed by either washout of compound (wash) or continuous exposure to compound (contin) for 1, 24, 48, 72 and 144 h. Live cells were counted by trypan blue exclusion. The number of viable cells (trypan blue negative) is graphed as the percentage of viable cells/ml normalized to the DMSO control. Data are representative of two independent experiments. (B) A549 cells were incubated with doxorubicin (50 nM) or disorazole C_1 (2 or 10 nM) for 24 h (open bars) or 48 h (black bars) and apoptosis determined with a TUNEL assay. N=3, bars are SEM.

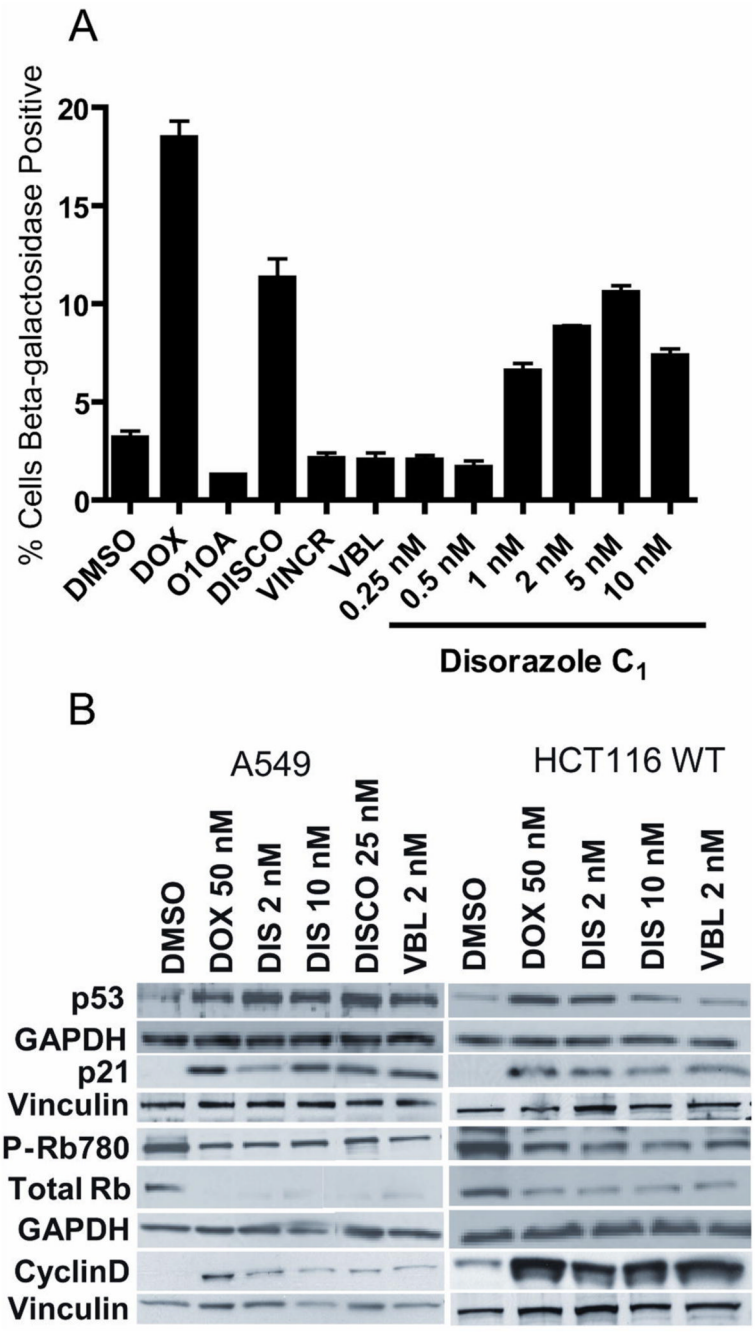

Figure 6. Disorazole C_1 causes premature senescence

(A) A549 cells were treated for 7 days with disorazole C_1, IC_{50} concentrations of discodermolide (DISCO; 25 nM), vincristine (VINCR; 20 nM) or vinblastine (VBL; 2 nM) followed by β-galactosidase staining, which was quantified using the brightfield module and compartmental bioapplication analysis on the ArrayScan VTI with values representative of at least two independent experiments. Doxorubicin (DOX; 50 nM) was used as a positive control for senescence while DMSO vehicle and the inactive analog O1OA (10 nM) were used as negative controls. (B) A549 and HCT116 cells were treated for 7 days and cell lysates were probed by Western blot analysis of protein markers of senescence. GAPDH and vinculin, which were used as loading controls, are located directly below the examined protein lanes.

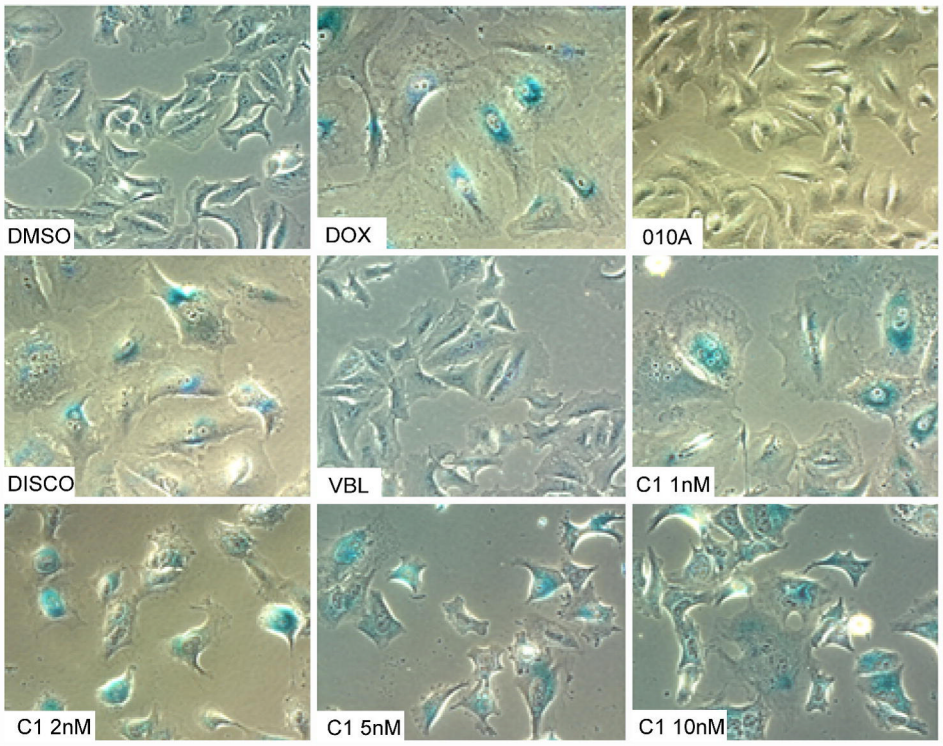

Figure 7. Disorazole C_1 causes premature senescence

A549 cells were treated for 7 days with vehicle (DMSO), doxorubicin (DOX, 50 nM), the inactive analog 010A (10 nM), discodermolide (DISCO, 25 nM) vinblastine (VBL, 2 nM), or disorazole C_1 (C_1, 1–10 nM) followed by β-galactosidase staining.

Table 1

Growth inhibition with microtubule disrupting agents

Human cells were plated in 96-well plates, allowed to attach for 24 h and treated for 72 h with DMSO or a range of concentrations of test agents. Cell number was determined spectrophotometrically at 570 nm minus absorbance at 690 nm after exposure to 3-(4,5- dimethylthiazol-2-yl)-2,5-diphenyltetrazolium bromide (MTT) or by measuring fluorescence (excitation = 560, emission = 590) in live cells using the Cell Titer Blue Assay (Promega, Madison, WI).

Cell Line	Description	IC_{50} (nM) ± SEM[a]		
		Disorazole C_1	Vincristine	Vinblastine
A549	Lung carcinoma	2.21 ± 0.23	21.62 ± 2.68	1.52 ± 0.09
PC-3	Prostate adenocarcinoma carcinoma	1.57 ± 0.10	4.68 ± 0.29	0.86 ± 0.08
MDA-MB-231	Breast epithelial adenocarcinoma	3.53 ± 0.19	7.16 ± 0.37	1.34 ± 0.21
2008	Ovarian carcinoma	1.91 ± 0.23	21.81 ± 2.92	2.24 ± 0.16
HCT116	Colorectal carcinoma	1.09 ± 0.41	5.62 ± 0.33	1.40 ± 0.07
UPCI:SCC104	Oral squamous carcinoma	6.87 ± 0.54	2.98 ± 0.22	1.13 ± 0.18
PCI 15A	Head and neck squamous carcinoma	0.26 ± 0.03	0.41 ± 0.04	1.86 ± 0.14
PCI 15B	Head and neck squamous carcinoma	0.34 ± 0.03	0.94 ± 0.20	1.81 ± 0.27
PCI 37A	Head and neck squamous carcinoma	0.53 ± 0.07	0.66 ± 0.06	2.51 ± 0.06
PCI 37B	Head and neck squamous carcinoma	0.26 ± 0.02	0.49 ± 0.05	3.58 ± 0.45
UMSCC22A	Head and neck squamous carcinoma	0.40 ± 0.06	1.45 ± 0.24	3.27 ± 0.70
WI-38 Confluent	Fibroblasts	>100	ND	>100
WI-38 Proliferating	Fibroblasts	1.74 ± 0.78	8.58 ± 0.78	1.54 ± 0.13

[a] IC_{50} values are mean of 8 determinations.